

Article

Experimental Investigation of the Effects of Grooves in Fe₂O₄/Water Nanofluid Pool Boiling

Marwa khaleel Rashid ¹, Bashar Mahmood Ali ^{2,*} , Mohammed Zorah ^{3,4} and Tariq J. Al-Musawi ⁵¹ Renewable Energy Research Center—Kirkuk, Northern Technical University, Kirkuk 36001, Iraq² Department of Construction Engineering and Project Management, College of Engineering, Alnoor University, Mosul 41012, Iraq³ Department of Computer Technology Engineering, Imam Al-Kadhumi College, Baghdad 00964, Iraq⁴ Department of Civil Engineering, Mazaya University College, Nasiriyah 64001, Iraq⁵ Building and Construction Techniques Engineering Department, College of Engineering and Engineering Techniques, Al-Mustaqbal University, Babylon 51001, Iraq

* Correspondence: bashar.m@alnoor.edu.iq

Abstract: In this study, we systematically explored how changing groove surfaces of iron oxide/water nanofluid could affect the pool boiling heat transfer. We aimed to investigate the effect of three types of grooves, namely rectangular, circular, and triangular, on the boiling heat transfer. The goal was to improve heat transfer performance by consciously changing surface structure. Comparative analyses were conducted with deionized water to provide valuable insights. Notably, the heat transfer coefficient (HTC) exhibited a significant increase in the presence of grooves. For deionized water, the HTC rose by 91.7% and 48.7% on circular and rectangular grooved surfaces, respectively. Surprisingly, the triangular-grooved surface showed a decrease of 32.9% in HTC compared to the flat surface. On the other hand, the performance of the nanofluid displayed intriguing trends. The HTC for the nanofluid diminished by 89.2% and 22.3% on rectangular and triangular grooved surfaces, while the circular-grooved surface exhibited a notable 41.2% increase in HTC. These results underscore the complex interplay between groove geometry, fluid properties, and heat transfer enhancement in nanofluid-based boiling. Hence, we thoroughly examine the underlying mechanisms and elements influencing these observed patterns in this research. The results provide important insights for further developments in this area by shedding light on how surface changes and groove geometry may greatly affect heat transfer in nanofluid-based pool boiling systems.

Keywords: heat transfer coefficient; pool boiling; nanofluid; grooved surface; optimal heat flux



Citation: Rashid, M.k.; Ali, B.M.; Zorah, M.; Al-Musawi, T.J. Experimental Investigation of the Effects of Grooves in Fe₂O₄/Water Nanofluid Pool Boiling. *Fluids* **2024**, *9*, 110. <https://doi.org/10.3390/fluids9050110>

Academic Editor: Carlos A. Nieto De Castro

Received: 24 March 2024

Revised: 4 May 2024

Accepted: 6 May 2024

Published: 8 May 2024



Copyright: © 2024 by the authors. Licensee MDPI, Basel, Switzerland. This article is an open access article distributed under the terms and conditions of the Creative Commons Attribution (CC BY) license (<https://creativecommons.org/licenses/by/4.0/>).

1. Introduction

Recently, many studies have been conducted in pool boiling because of its many applications in the industry. The most common boiling applications are condensers, boilers, heat pumps, nuclear reactors, electronic chip cooling, and air conditioning systems. In order to develop the heat transfer capabilities of pool boiling, a number of alternatives could be utilized, namely adding nanoparticles or a surface activator to the base fluid, expanding the heating surface, applying an electric or magnetic field, and vibrating the thermal surface [1].

A colloidal solution of magnetic nanoparticles, namely iron, cobalt, iron oxide, gamma iron oxide, and cobalt oxide, which are completely stable in a base fluid, is called ferrofluid. The idea of using nanofluids in heating systems was first proposed by Choi [2]. Parameters such as nanoparticle concentration, nanoparticles size and type, surface roughness, the contact angle of bubbles, system pressure, etc., complicate the boiling mechanism.

Numerous studies have been devoted to nanofluids pool boiling [3–9]. Chandra et al. [10] studied copper/water at concentrations of 0.25%, 0.5%, and 1% by weight on a 30 mm² steel surface. They observed nanofluid had a higher critical heat flux than

water, and the HTC decreased with increasing nanoparticles. Hia [11] studied water and aluminum oxide/water behaviour on a variety of surfaces. He observed a development in HTC of rough heater surface. Also, studying the nanoparticle concentration, a boiling test at two concentrations of 0.1% and 0.01% by volume was performed on a rough surface. According to the results, in high heat fluxes, with increasing concentration, the HTC decreases because of the tendency of the particles to clump. Shi et al. [12] studied aluminum oxide/water on copper heaters and found that the boiling HTC increased. In other research, methods such as tri-hybrid nanofluid [13] and using vortex generation for improving heat transfer [14] have been examined.

Norouzpour et al. [15] examined the effects of nanoparticle size on pool boiling. They found that by augmenting the nanoparticle diameter, the HTC increased. Generally, they reported a drop in HTC compared to pure water. Some researchers have also reported no considerable change in the HTC of the nanofluid boiling. For example, Vassallo et al. [16] investigated the 0.5% volumetric silicon oxide nanofluid on a nickel–chromium horizontal wire. In their results, little change in boiling HTC was observed.

Since surface finish could significantly affect pool boiling, a number of papers have been devoted to surface roughness, surface expansion, geometry change, and surface position. Hachem et al. [17] performed a comparative study of the HTC of water on a smooth and porous surface. They reported an increase in the HTC. This is because cavities increase nucleation site density and cause bubbles to form at lower surface temperatures. In another study, Das et al. [18] used surfaces with different structures to increase the HTC of water. These surfaces consisted of a number of parallel or intersecting grooves. They found that grooved surfaces improved the pool boiling of pure water due to their higher thermal surface. Also, Alimoradi et al. [19,20] studied the effects of surface modification on pool boiling. Pastuszko et al. [21] experimented with finned surfaces for water. A copper coating with micro-holes is attached to the fins. Their results show that at high fluxes, the finned surface with a fin of 1 mm height has the greatest effect on the HTC. Dadjoo et al. [22] carried out research on the effect of silicon oxide/water nanofluid surface on the copper heater and found that, as slope increases, the HTC of boiling decreases. In their study, bubbles form on the boiling surface and join with each other, which increases thermal resistance. In another study, researchers [23,24] proposed a boiling method for surface modification. Umesh et al. [25] studied pentane and pentane/copper oxide on a smooth and expanded surface at atmospheric pressure. The expanded surfaces were two levels with small and large fins. The HTC of pentane on the surface of the small fin increased by 10–15%, and on the surface of the large fin it decreased by 5–10%. They stated that because of the formation of more cracks during grooving and the capillary effect of the fluid, the HTC at the small fins increased, and on large fins, due to the lateral surface of the fins, more resistance to bubble separation from the surface was found. Further, in their results, it has been seen that the HTC of pentane/copper oxide on the surface of the fin was increased by about 15–25%, and for a concentration of 0.01%, it is almost equal to the boiling of pentane. This is because at higher concentrations a micro-layer forms under the growing bubble, blocking the nucleation sites. Narayan et al. [26] studied aluminum oxide/water nanofluid on rough surfaces. They used the nanoparticle surface interaction parameter (φ) as the criterion for their results. When $\varphi \leq 1$, the HTC decreases. Because the nanoparticles block the nucleation sites and create additional thermal resistance. When this parameter is greater than one, the HTC increases at low concentrations.

Research has also been done on utilizing ferroalloys in pool boiling. Abdollahi et al. [27] studied a magnetic field applied on water/iron oxide. They found an optimum volumetric concentration of 0.1% for ferrofluid, which increased the HTC by 43% [28]. Abdollahi et al. [29], in another study, studied time and surface modifications in the iron oxide/water pool boiling process and found that heat transfer on deposited surfaces decreased with low heat flux and increased with high heat flux. Lee et al. [30] compared the critical heat flux (CHF) of a ferrofluid with a water-based fluid, aluminum oxide/water, and titanium oxide/water. In their results, it was seen that nanoparticles increased the

critical heat flux of boiling, and the highest CHF was related to ferrofluid and was 2.6 times higher than pure water. This is because of the accumulation of nanoparticles on the surface and increased surface wettability [31].

According to previous research, despite the fact that there is research on the use of nanofluids in pool boiling, few studies have been conducted on heated and grooved surfaces. In the present paper, the effect of rectangular, circular, and triangular grooved surfaces on the pool boiling of ionized water and iron oxide/water is investigated experimentally. Consequently, the pool boiling test of pure and ferrofluid was performed on a smooth surface and then on grooved surfaces. After which the depth of the grooves is increased, and its effect on heat transfer is investigated.

2. Materials and Methods

2.1. Preparation of Nanofluid

Nanofluids are prepared in two methods, one-stage and two-stage. In the first method, nanoparticles are produced directly in the fluid. However, in the later method, nanoparticles are dispersed in the form of dry powders in the fluid. The benefit of the first method is that the size and distribution of nanoparticles are controlled, and the stability of nanofluid in this method is higher than in the two-stage method.

To achieve stable nanofluids, methods such as ultrasonic rippling, acidification, and the addition of surfactants are used. The ultrasonic ripping method breaks the nanoparticle masses and makes the solution uniform in a short time. Adding surfactants to the solution causes the solution to be uniform, but affects the thermophysical properties of the fluid and does not work well in high-temperature applications. The method of changing the acidity is a suitable method for stabilizing the nanofluid.

In this paper, iron oxide/water nanofluids are fabricated by a one-step method developed by Berger [32] and a surfactant is added to stabilize them. First, 1 mL of iron (II) chloride is mixed with 4 mL of iron (III) chloride. Then 2.64 mL of ammonia is added to 50 mL of deionized water and added to the solution with a syringe pump. Simultaneously, with the addition of ammonia, the solution is placed in a magnetic stirrer at a speed of 1000 rpm. After a few minutes, the iron oxide particles settle, and the water on top of the particles is removed. The resulting precipitate is then placed in a centrifuge for 5 min. After this step, a black deposit remains at the bottom of the container. The surfactant tetramethylammonium hydroxide is then added to the precipitate and placed on a magnetic stirrer at 500 rpm for half an hour. Finally, by removing excess ammonia, 1% by volume of iron oxide nanofluid is obtained. The prepared nanofluid is stable for at least one month, and no nanoparticles precipitate.

In order to get more insight of the nanofluid, dynamic light scattering (DLS) and transmission electron microscopy (TEM) tests are performed for the fabricated nanofluid. Figures 1 and 2 show the results of DLS and TEM tests for nanofluid, respectively. It is clear that the average diameter of nanoparticles is about 15 nm. To investigate the stability of our fluid, a potential test has also been performed. This test represents the magnitude of the electric charge at the nanoparticle surface. Many researchers [33–39] have reported that colloidal solutions are stable at zeta potentials greater than 30 mV. This value for the nanofluid made at a concentration of 0.01% was -31 mV, which indicates the high stability of the nanofluid [40–47].

Before each boiling test, a diluted solution with a concentration of 0.01% is placed in an ultrasonic waveguide with 400 watts and 24 kHz for half an hour.

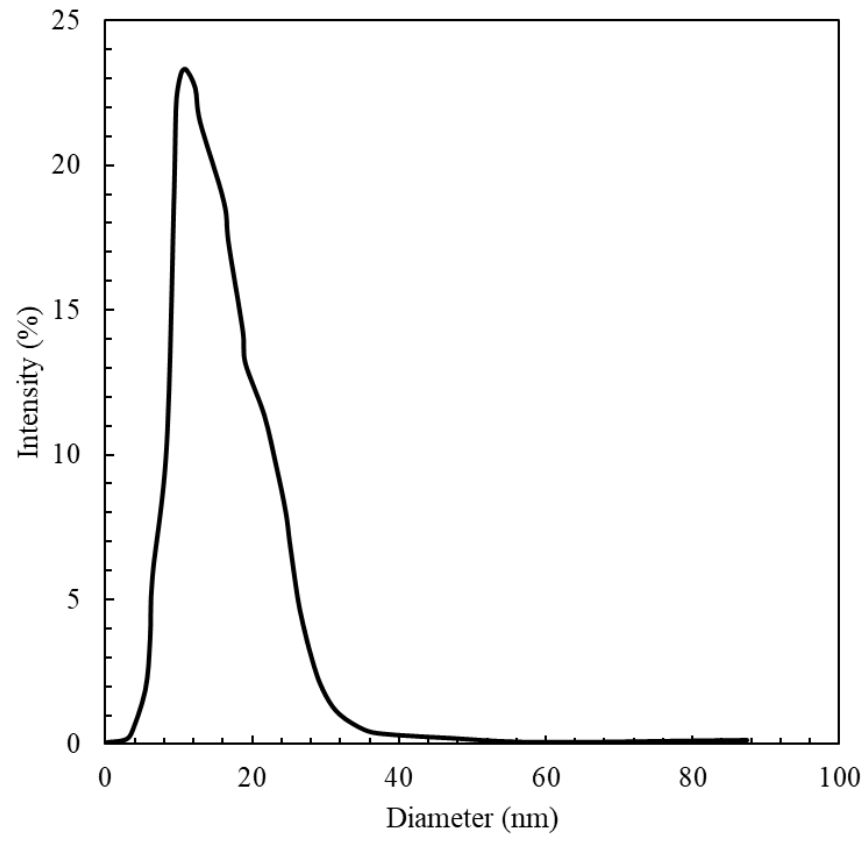


Figure 1. The DLS test for Fe₃O₄/water.

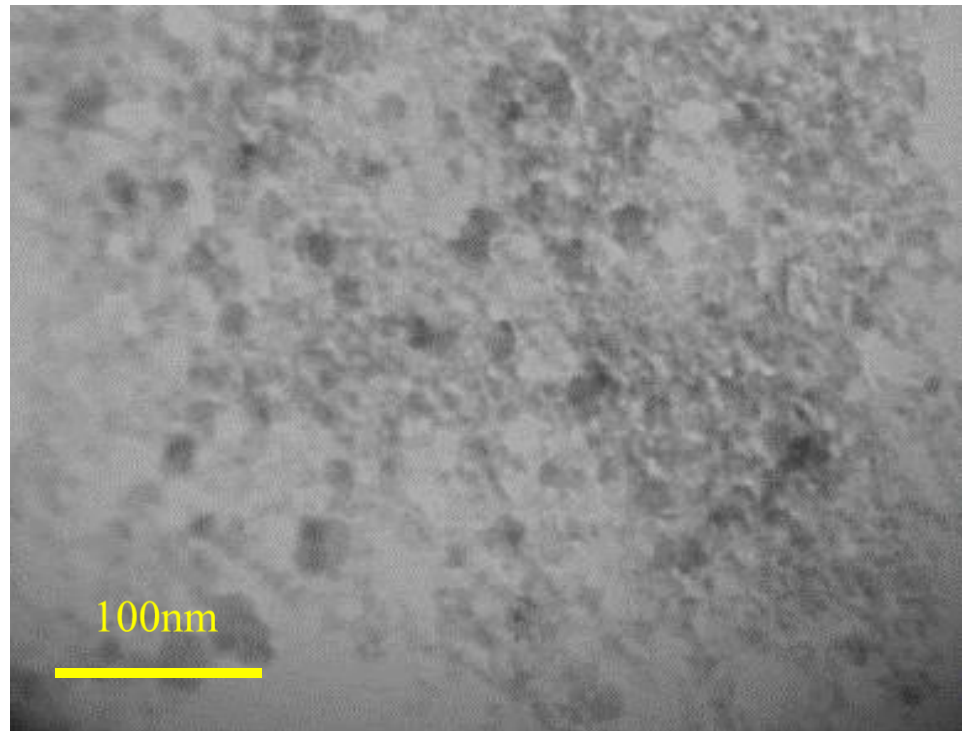


Figure 2. The TEM test for Fe₃O₄/water.

2.2. The Boiling System

The picture of the laboratory set made for the experiments is shown in Figure 3. The main components of the test apparatus are the copper and insulation heater set, boiling tank, condenser, and cooling system, voltage, current, and displays control system. The voltage regulator creates a constant voltage and current to generate a constant heat flux in the heater. The heater comprises two sections, namely heater cartridge and cooper block. The heater cartridge is inside the cooper block, and in the top section of the block, there are three thermocouples to record the temperature in the vicinity of the boiling surface. By using the thermocouples, the heat flux is calculated, the boiling surface temperature could be calculated as well. In the boiling vessel, there is a thermocouple to measure the bulk temperature of the fluid. By using these parameters, we are able to calculate the heat transfer coefficient. Additionally, in the top section of the boiling vessel, a condenser is installed to return the vapor to the vessel and keep the fluid volume constant.

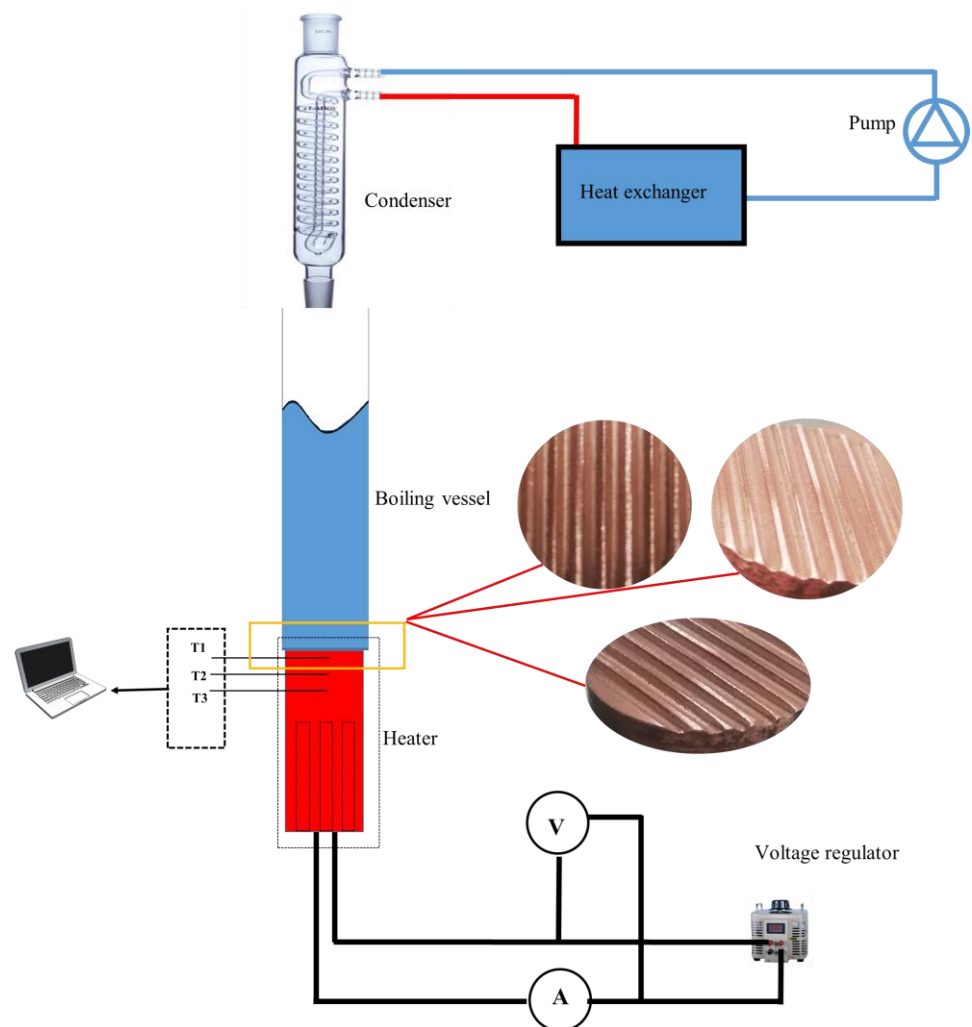


Figure 3. A schematic and real view of the experimental setup.

The cylindrical heater is made of 99.99% pure copper, and it has a diameter of 45 mm and a length of 110 mm. There are three holes in the heater, each of which has 10 mm diameter. These holes are 75 mm deep, and they are situated at relative 120°. At the end of the heater, the bullet elements are created for inserting cartridge elements. The heating elements with a power of 650 watts are 10 mm in diameter and 80 mm long. Also, three holes with a diameter of 4 mm and a depth of 22.5 mm at a distance of 8, 18, and 30 mm

from the surface of the heater with an angle of 120 degrees relative to each other are created by a honing machine to hold thermocouples.

The cylinder insulation is made of polytetrafluoroethylene (PTFE) whose inner and outer diameters are 45 mm and 100 mm, respectively. The lower part of the insulation is fastened to the upper part by three socket head cap screws and holds the copper heater. Three springs with a length of 38 mm have been used to eliminate the effect of the expansion of socket head cap screws due to the heat and also to eliminate the threads of the screw holes. In addition to PTFE insulation, a 20 mm thick elastomeric insulation is wrapped around the heater and the insulation assembly. The thermal conductivity of the heater, PTFE insulation, and elastomer are measured using KD_2 and are 400 W/K, 0.25 W/K, and 400 W/K, respectively. Radial conductive heat transfer can be neglected, and the thermal conductivity transferred to the surface of the heater can be considered one-dimensional.

The boiling tank is a cylinder made of Pyrex whose diameter, height, and thickness are 60 mm, 300 mm, and 5 mm, respectively. Moreover, it is glued to the insulation with Permatex glue. For sealing the tank and insulation, as well as the surface of the heater and insulation, two Whitney O-rings with a diameter of 59 and 40 mm, respectively, with a temperature tolerance of 250 °C, have been used.

A condenser has been used to condense the boiling vapors and keep the amount of boiling fluid constant. The condenser is made of Pyrex, which is 400 mm long, and its diameter is 50 mm. Teflon tape is used to seal the end of the condenser. To cool the circulating condenser, water is pumped at a rate of 21 mL/s from the water and ice tank and then returned to the tank. The water and ice tank temperature are 20 °C and is controlled by a mercury thermometer. Usually at the end of each boiling test at high heat fluxes, more ice molds are used due to the increase in circulating water temperature.

A voltage controller (Auto-trans) with a maximum of 300 volts is used to adjust the voltage and achieve the desired power at each stage of the boiling test. An ammeter is used to measure current with an accuracy of 0.1 amps, and a voltmeter is used to measure voltage with an accuracy of 1 volt. The thermocouples are 80 mm long and 4 mm in diameter and are of PT100 type, and have been calibrated by the oil bath method in the calibration laboratory. Also, the Autonics temperature display model has an accuracy of 0.1 degrees.

2.3. Boiling Surface

The smooth boiling surface has a diameter of 40 mm; before each test it is sanded with sanding sheets No. 400, 600, and 800 using a lathe, and then its roughness is measured by a roughness tester. The average surface roughness of the boiling surface in all experiments is 213 nm (Figure 4). Rectangular, circular, and triangular grooved surfaces are made by wire cutting and have roughness similar to the smooth surface. The surface inside the grooves is sanded manually at a uniform speed before each test. Figure 5 shows the grooved surfaces of the boiling surface.

2.4. Relationships between Surface Temperature and Heat Flux

All experiments were started at low heat flux, 53 volts, and 2 amps. After boiling the fluid, the temperatures, voltage, and current are read, and the voltage of the device is added by the 5-volt voltage controller. Then the data is recorded after 5 min when the temperatures of the thermocouples are fixed. After the current reaches 6 amps, before the phenomenon of critical heat flux (CHF), the voltage is slowly reduced, and then the system is cut off. The amount of heat flux is calculated from Equations (1) and (2). The amount of heat loss is equal to the difference between the two values of heat flux obtained from Equations (1) and (2), which was less than 5% in all experiments.

$$q = K \frac{T_2 - T_1}{\Delta x_2} \quad (1)$$

$$q = \frac{VI}{\pi D^2/4} \quad (2)$$

In Equations (1) and (2), k is the thermal conductivity of the copper heater, and T_1 and T_2 are the temperature of thermocouples 1 and 2 at a distance of 8 and 18 mm from the boiling surface, respectively. ΔX_2 is the distance between the two holes of the thermocouples. V , I , and D are the voltage, the electric current, and the diameter of the heater.

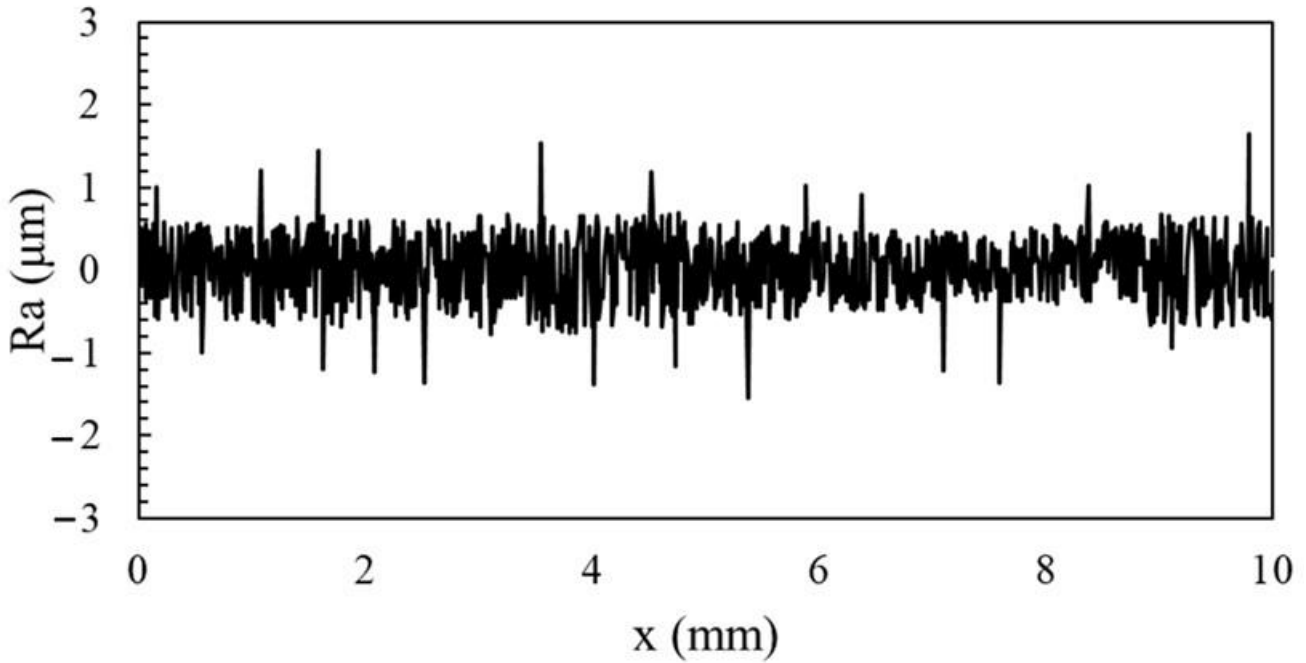


Figure 4. The heater surface’s roughness profile.

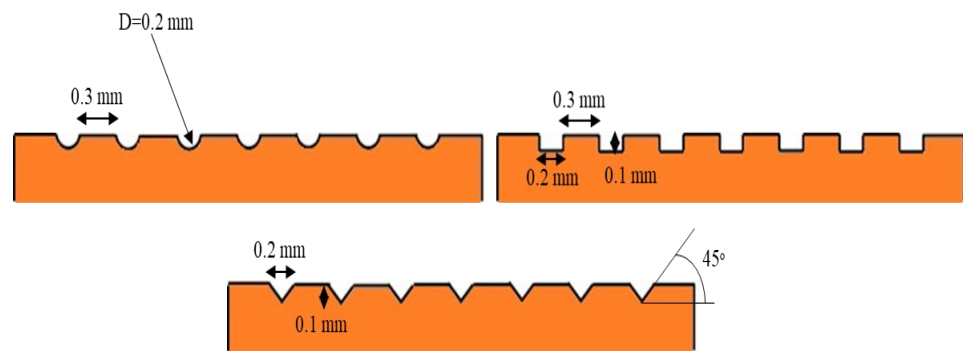


Figure 5. Grooved surfaces representation.

The surface temperature is calculated by extrapolating the temperatures T_1 and T_2 due to the one-dimensional conductive heat transfer (Equation (3)). The HTC is obtained from Equation (4). ΔX_1 is the distance between thermocouple number 1 and the boiling point, and T_{sat} is the saturation temperature of the fluid.

$$T_w - T_{sat} = T_1 - \frac{\Delta X_1}{\Delta X_2}(T_2 - T_1) - T_{sat} \tag{3}$$

$$h = \frac{q}{T_w - T_{sat}} \tag{4}$$

2.5. Uncertainty Analysis

In this research, the Holman method [48] is utilized for uncertainty analyses. In this method, if the parameter F is a function of the variables x_1, x_2, \dots, x_n , then its uncertainty value is obtained from Equation (5). U is the amount of measurement error.

$$\frac{U_F}{F} = \left[\sum_{i=1}^n \left(\frac{U_{x_i}}{x_i} \right)^2 \right]^{0.5} \tag{5}$$

Therefore, the amount of heat flux uncertainty, surface and fluid temperature difference, and HTC are obtained from Equations (6)–(8), respectively. For all experiments, the highest heat flux uncertainty and HTC were 5.1 and 6.87%, respectively.

$$\frac{U_{q''}}{q''} = \sqrt{\left(\frac{U_k}{k} \right)^2 + \left(\frac{U_{(T_2-T_1)}}{T_2 - T_1} \right)^2 + \left(\frac{U_{\Delta x_2}}{\Delta x_2} \right)^2} \tag{6}$$

$$\frac{U_{(T_w-T_{sat})}}{(T_w - T_{sat})} = \sqrt{\left(\frac{U_{\Delta x_1}}{\Delta x_1} \right)^2 + \left(\frac{U_{(T_2-T_1)}}{T_2 - T_1} \right)^2 + \left(\frac{U_{\Delta x_2}}{\Delta x_2} \right)^2} \tag{7}$$

$$\frac{U_h}{h} = \sqrt{\left(\frac{U_q}{q} \right)^2 + \left(\frac{U_{(T_w-T_{sat})}}{(T_w - T_{sat})} \right)^2} \tag{8}$$

3. Results

In each experiment, 150 mL of deionized water or nanofluid is added into the boiling chamber, and experiments are in the pre-CHF range. The laboratory temperature is 20 °C, and the ambient pressure is 623 mmHg. To ensure accuracy and repeatability, each experiment was performed three times in three days under the same conditions.

3.1. Accuracy of Results

Boiling of deionized water was performed on a flat surface, and its data was compared with the proposed equation of Rohsenow [49], Equation (9). In this equation, $h_{fg}, \sigma, \rho_l, \rho_v, Pr, C_{p,l}$, and μ_l are the latent boiling heat, surface tension, density of liquid, density of vapor, Prandtl number, the specific heat capacity of water, and the viscosity of liquid, respectively. C_{sf} and n are 0.013 and 1 for smooth cooper surface, respectively.

$$T_w - T_{sat} = \frac{h_{fg} C_{sf}}{c_{p,l}} \left[\frac{q}{\mu_l h_{fg}} \left(\frac{\sigma}{g(\rho_l - \rho_v)} \right)^{0.5} \right]^{\frac{1}{3}} Pr^n \tag{9}$$

Figure 6 shows the deionized water boiling curve and the Rohsenow’s curve, and there is a good correlation between the deionized water reference data [49]. Heat flux uncertainty is also shown in Figure 6.

3.2. Ferrofluid Boiling of Iron Oxide/Water on the Surface of the Smooth Heater

Boiling tests were performed for 0.01% volumetric iron oxide/water ferrofluid on a smooth surface. The diagram of heat flux in terms of excess temperature and HTC in terms of heat flux of iron oxide/water ferrofluid in comparison with deionized water is seen in Figure 7.

The saturation temperature of nanofluid is 96 °C. According to Figure 7, in all heat fluxes, the ferrofluid boiling diagram is shifted to the left, meaning that at the same heat flux, a smaller excess temperature difference is required. The HTC of nanofluid boiling

relative to water increased by an average of 25.9%. This value is the average percentage increase of the boiling HTC results obtained from Equation (10).

$$\Delta h = \frac{h_{nf} - h_w}{h_w} \times 100 \tag{10}$$

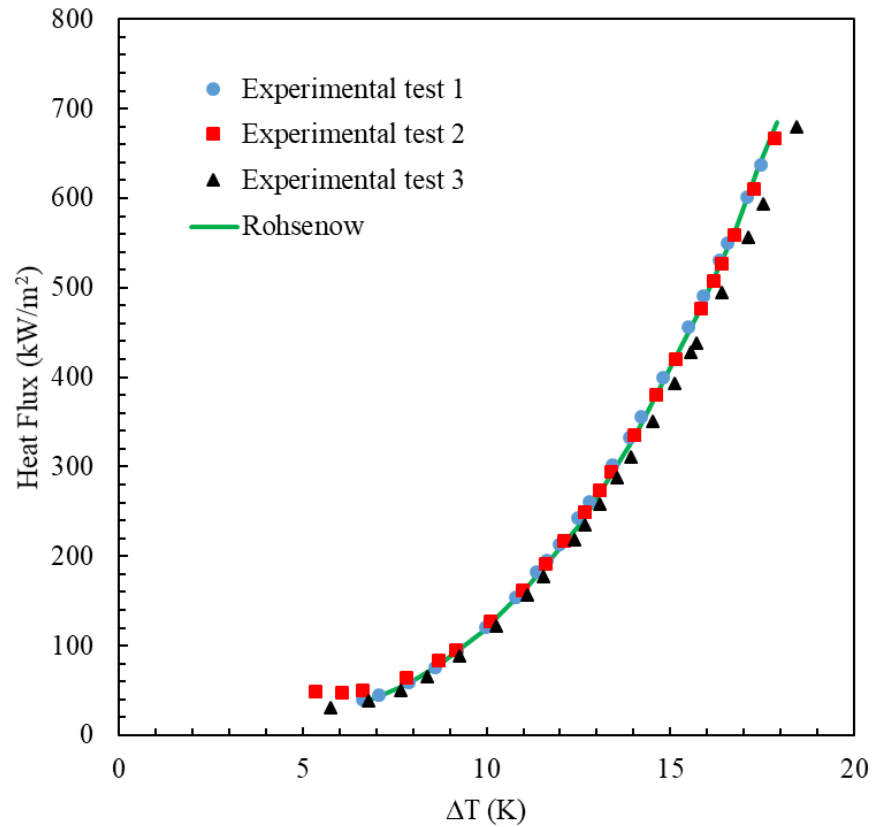


Figure 6. The deionized water and Rohsenow’s results.

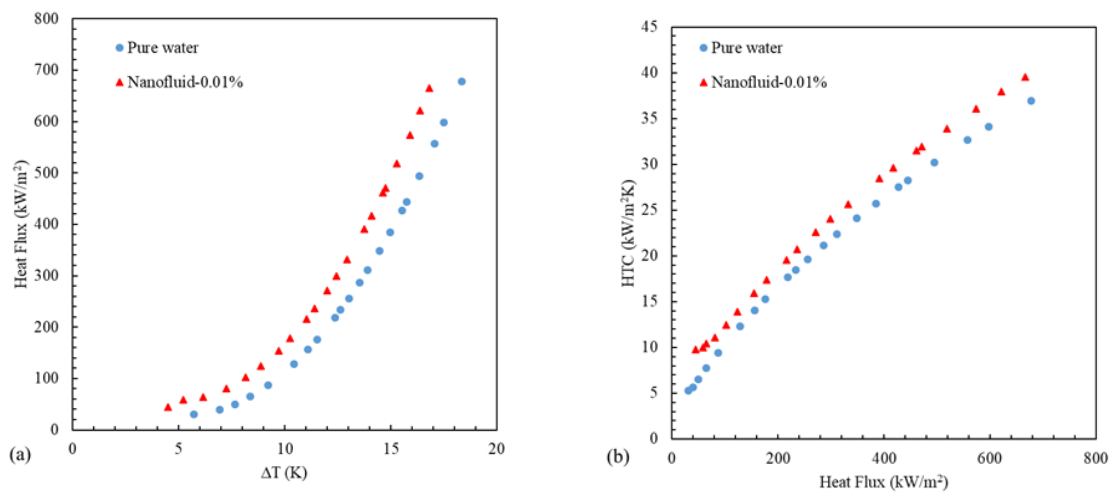


Figure 7. The results of pure water and 0.01% volumetric nanofluid; (a) heat flux with respect to superheat temperature and (b) HTC with respect to heat flux.

In Equation (10), h_{nf} and h_w are the nanofluid and water HTC, respectively. The reason for the improvement of heat transfer can be considered the high thermal conductivity of nanoparticles. Further, due to the average surface roughness (213 nm), and the average diameter of nanoparticles (15 nm), the value of the nanoparticle surface interaction parameter (φ) is greater than one, which increases the HTC of the nanofluid.

3.3. Boiling Deionized Water on Grooved Surfaces

In this section, the deionized water boiling test was performed on three types of rectangular, circular, and triangular grooved surfaces, which can be seen in Figure 8. Boiling water on the surfaces with circular and triangular grooves had the highest and lowest HTC, respectively. The average HTC in boiling deionized water on the surfaces with circular and rectangular grooves increased by 91.5% and 48.7%, respectively; additionally, on the surface with triangular grooves, it decreased by 32.9%. It is assumed that this result is due to the unique geometry of these grooves, which can prevent proper bubble propagation and fluid flow. The sharp angles and corners of triangular grooves are likely to trap bubbles and cause local thermal resistance, which reduces heat transfer. In addition, nanoparticles have the potential to amass substantially in these corners, creating an insulating layer that impedes the passage of heat. Additional experimental investigations are planned to study this matter.

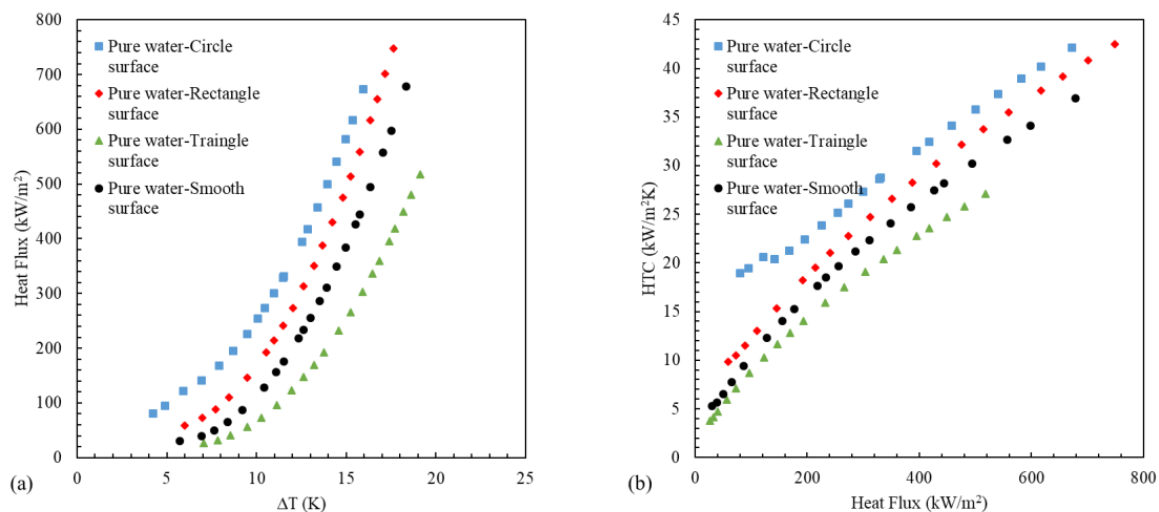


Figure 8. The results of pure water in different heater surfaces; (a) heat flux with respect to superheat temperature and (b) HTC with respect to heat flux.

The areas of the central groove in rectangular, circular, and triangular surfaces are 1.6 cm^2 , 1.256 cm^2 , and 1.12 cm^2 , respectively. Although the area of a rectangular grooved surface is larger than a circle, due to the difference in the geometry of the groove, the boiling heat transfer on the circular grooved surface is improved. According to the results of Dadjoo et al. [22], by changing the position of the heater surface from horizontal to vertical, the intensity of boiling heat transfer decreases. In fact, the surface wettability on the vertical wall of the groove is less than the horizontal surface, because the contact angle of the bubble in the vertical surface is greater than the horizontal. In this paper, half of the surface of the rectangular groove is in the vertical position [50–55]. Also, in the rectangular groove, the presence of corners makes it more difficult to separate the bubbles from the surface. In a triangular groove, due to the slipping of bubbles and their accumulation in the center of the groove, the thermal resistance increases and the HTC decreases compared to deionized water.

3.4. Boiling of Iron Oxide/Water Nanofluid on Grooved Surfaces

A pool boiling test of 0.01% iron oxide/water nanofluid was also performed on grooved surfaces, the results of which can be seen in Figure 9. Due to the increase in surface area in grooved surfaces compared to the smooth surface, it is expected that the boiling heat transfer on the grooved surface will improve, but in rectangular and triangular grooved surfaces, the results have been contrary to expectations. HTC increased on average in ferrofluid boiling on the surface with the circular groove by 41.2%, but the percentage has decreased in rectangular and triangular surfaces by 22.3 and 89.2, respectively, compared to the smooth surface. The reason for this result can be considered to be increased accumulation of nanoparticles in the corners of the rectangular and triangular grooves and the formation of micro-layers under the bubbles, which clogs the nucleation sites and reduces the HTC. Easier separation of bubbles in circular grooves also improves heat transfer [56–58].

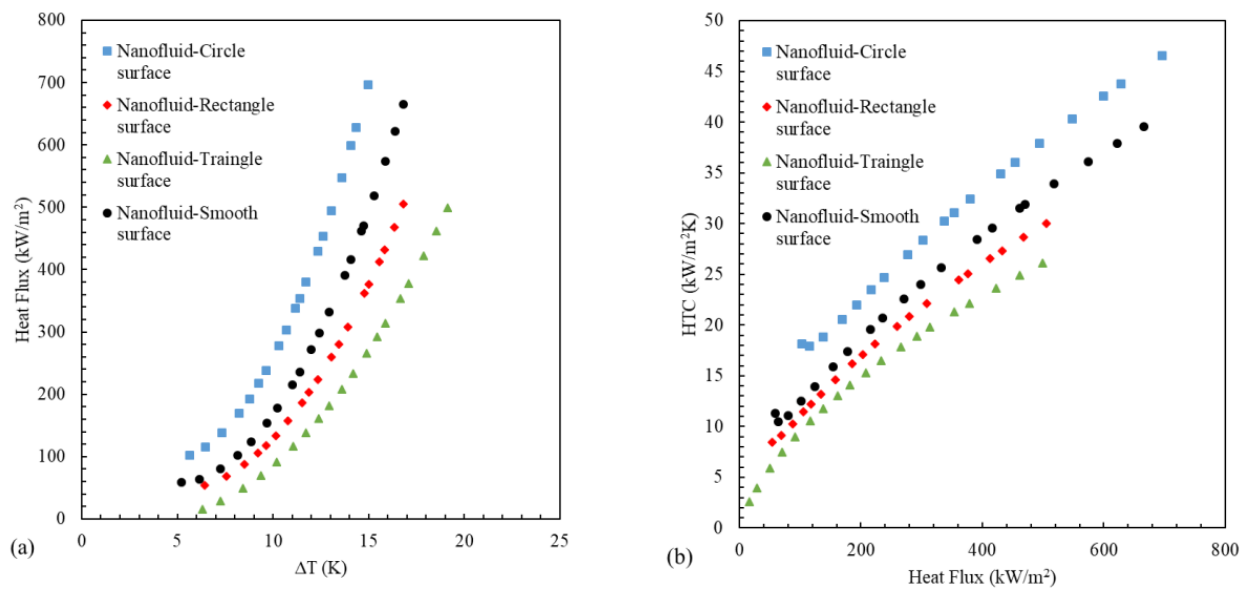


Figure 9. The results of 0.01% volumetric nanofluid in different heater surfaces; (a) heat flux with respect to superheat temperature and (b) HTC with respect to heat flux.

3.5. Effect of Groove Depth of Grooved Surfaces on Boiling of Water and Iron Oxide/Water Nanofluid

The depth of grooves in the grooved surfaces was increased from 1 mm to 2 mm by wire cutting. The roughness of the surfaces is the same as in the previous levels. Boiling experiments of deionized water and iron oxide/water nanofluid were performed on grooved surfaces with greater depth, which is shown in Figures 10 and 11 of their boiling curves, respectively. According to Figures 10 and 11, increasing the depth of the grooves has improved the boiling heat transfer of both water and nanofluid.

The average HTC of deionized boiling water on rectangular, circular, and triangular grooved surfaces with a depth of 2 mm has increased by 19.1%, 12.4%, and 42.9%, respectively, compared to a depth of 1 mm. In iron oxide/water nanofluid boiling, the average HTC of boiling in rectangular, circular, and triangular grooved surfaces has increased by 41.2%, 22.3%, and 41.4%, respectively, with increasing depth. As depth increases, the heat transfer surface area increases, the density of the nucleation sites increases, and the number of bubbles formed increases. In addition, when adding depth by wire cutting, the cracks in the grooves increase, which adds to the number of nucleation sites.

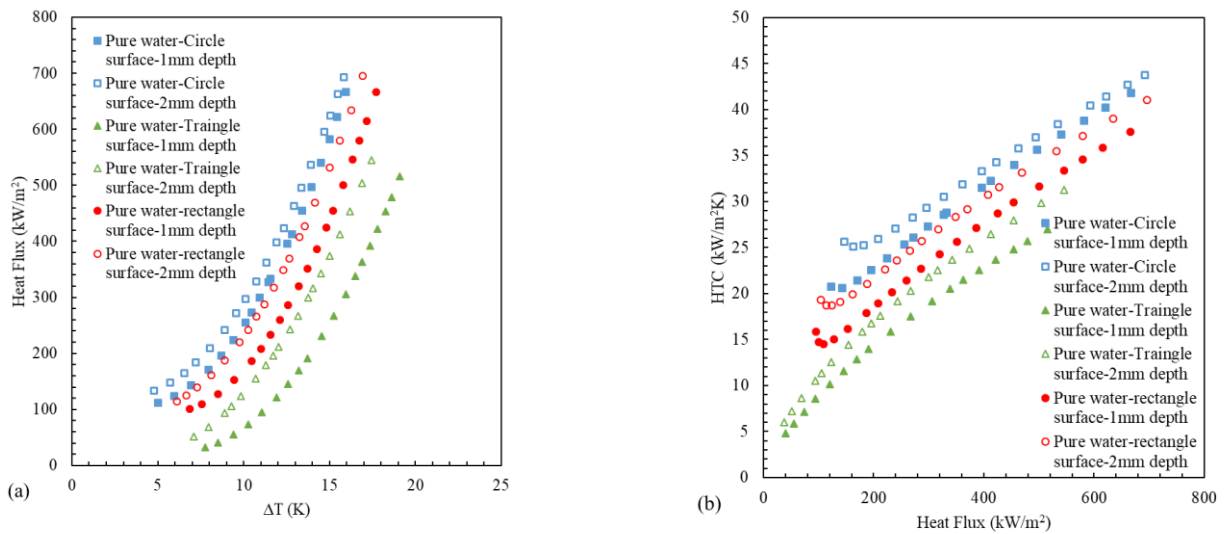


Figure 10. The accumulated results of the pure water; (a) heat flux with respect to superheat temperature and (b) HTC with respect to heat flux.

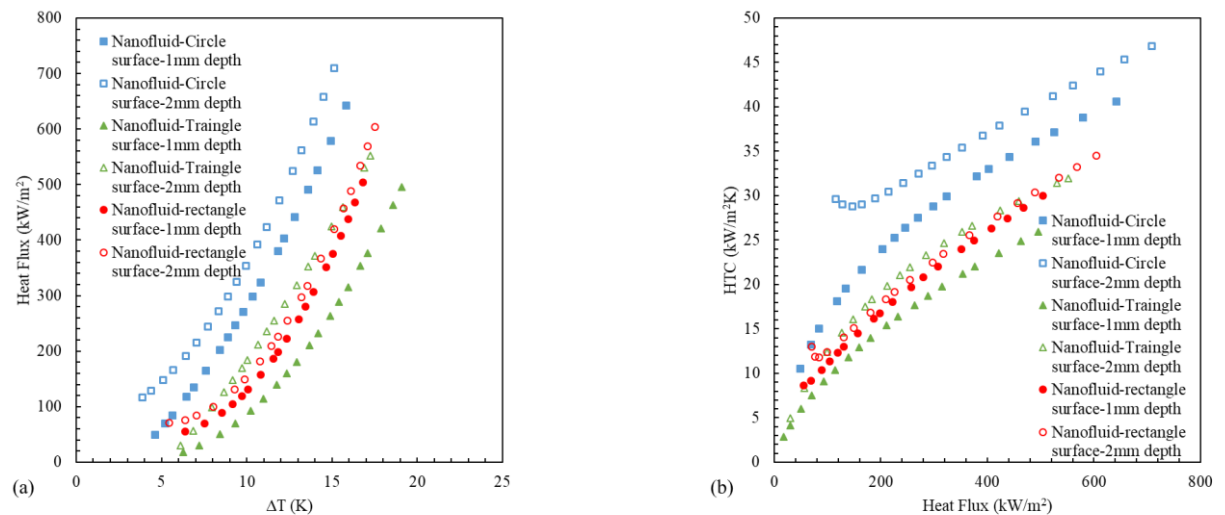


Figure 11. The accumulated results of the 0.01% volumetric nanofluid; (a) heat flux with respect to superheat temperature and (b) HTC with respect to heat flux.

Groove geometry has a significant effect on the heat transfer efficiency of the fluid flow. In particular, the circular groove utilizes the symmetry and, therefore, demonstrates a better heat transfer and bubble release performance. However, in the case of triangular grooves, as there are sharp corners which could trap bubbles, a considerable thermal resistance is created [59–61]. Therefore, in that case, the heat transfer coefficient drops at a significant rate.

Our research demonstrates that using various groove geometry could substantially affect the heat transfer rate and critical heat flux. In particular, in the case of circular grooved surfaces, the heat transfer has increase significantly because of the better bubble behavior in these grooves. However, for triangular grooves, the mentioned problems would cause a drop in the HTC.

4. Conclusions

In this paper, boiling of deionized water and nanofluid of iron oxide/water with a volumetric concentration of 0.01% on smooth surfaces and grooved surfaces has been investigated experimentally. The use of nanofluid improves the HTC, provided that

the surface-nanoparticle interaction parameter is greater than one, and the nanofluid is completely stable. The type and depth of grooves also affect the boiling results.

The most important results of the experiments are:

- In boiling deionized water on grooved surfaces, the surface with circular and rectangular grooves improves heat transfer, and the surface with triangular grooves reduces the heat transfer rate compared to the smooth surface. In a triangular groove, the thermal resistance increases due to the accumulation of bubbles in the center of the groove.
- The HTC in ferrofluid boiling increased on circular grooved surfaces and decreased on rectangular and triangular grooved surfaces due to the deposition of more nanoparticles in rectangular and triangular grooves than in circular ones due to the presence of groove corners.

By increasing the depth of the grooves, due to the increase of the heater surface, the boiling heat transfer rate of both water and ferrofluid has increased.

Author Contributions: M.k.R.: Resources, Investigation, Methodology, Investigation, Funding acquisition. B.M.A.: reviewing & editing, Methodology, Investigation, Conceptualization, Validation, Writing—original draft, Writing—review & editing. M.Z. and T.J.A.-M.: Conceptualization, Investigation, Visualization, Writing—review & editing, Resources. All authors have read and agreed to the published version of the manuscript.

Funding: The current work have no received external support, and APC was funded by Alnoor university.

Data Availability Statement: The data presented in this study are available on request from the corresponding author.

Acknowledgments: The authors would like to thankful Alnoor University for supporting this work.

Conflicts of Interest: The authors declares no conflicts of interest.

Nomenclature

| | |
|----------|--|
| C_{sf} | Pressure correction coefficient |
| h | Enthalpy (J/kg) |
| H | Heat transfer coefficient (W/m^2K) |
| I | Current (A) |
| K | Thermal conductivity (W/mK) |
| P | Pressure (Pa) |
| q | Heat flux (W/m^2) |
| R_a | Mean roughness (μm) |
| T | Temperature (K) |
| U | Uncertainty |
| V | Voltage (v) |

Greek letters

| | |
|----------|---------------------------------|
| μ | Viscosity (N/m^2) |
| ρ | Density ($kg\ m^{-3}$) |
| σ | Surface tension ($N\ m^{-1}$) |

Subscripts

| | |
|-------|------------|
| l | Liquid |
| sat | Saturation |
| v | Vapor |

References

1. Bergles, A.E. Enhancement of pool boiling. *Int. J. Refrig.* **1997**, *20*, 545–551. [[CrossRef](#)]
2. Choi, S. Enhancing thermal conductivity of fluids with nanoparticles. *ASME-FED* **1995**, *231*, 99–106.
3. Kamel, M.S.; Lezsovits, F. Enhancement of pool boiling heat transfer performance using dilute cerium oxide/water nanofluid: An experimental investigation. *Int. Commun. Heat Mass Transf.* **2020**, *114*, 104587. [[CrossRef](#)]
4. Tian, Z.; Etedali, S.; Afrand, M.; Abdollahi, A.; Goodarzi, M. Experimental study of the effect of various surfactants on surface sediment and pool boiling heat transfer coefficient of silica/DI water nano-fluid. *Powder Technol.* **2019**, *356*, 391–402. [[CrossRef](#)]

5. Eskandari, E.; Alimoradi, H.; Pourbagian, M.; Shams, M. Numerical investigation and deep learning-based prediction of heat transfer characteristics and bubble dynamics of subcooled flow boiling in a vertical tube. *Korean J. Chem. Eng.* **2022**, *39*, 3227–3245. [[CrossRef](#)]
6. Smaisim, G.F.; Abed, A.M.; Al-Madhhachi, H.; Hadrawi, S.K.; Al-Khateeb HM, M.; Kianfar, E. RETRACTED ARTICLE: Graphene-Based Important Carbon Structures and Nanomaterials for Energy Storage Applications as Chemical Capacitors and Supercapacitor Electrodes: A Review. *BioNanoScience* **2023**, *13*, 219–248. [[CrossRef](#)]
7. Roodbari, M.; Alimoradi, H.; Shams, M.; Aghanajafi, C. An experimental investigation of microstructure surface roughness on pool boiling characteristics of TiO₂ nanofluid. *J. Therm. Anal. Calorim.* **2022**, *147*, 3283–3298. [[CrossRef](#)]
8. Alimoradi, H.; Eskandari, E.; Pourbagian, M.; Shams, M. A parametric study of subcooled flow boiling of Al₂O₃/water nanofluid using numerical simulation and artificial neural networks. *Nanoscale Microscale Thermophys. Eng.* **2022**, *26*, 129–159. [[CrossRef](#)]
9. Ahmad, S.; Takana, H.; Ali, K.; Akhtar, Y.; Hassan, A.M.; Ragab, A.E. Role of localized magnetic field in vortex generation in tri-hybrid nanofluid flow: A numerical approach. *Nanotechol. Rev.* **2023**, *12*, 20220561. [[CrossRef](#)]
10. Chandra, R.; Kathiravan, R. Pool boiling characteristics of multiwalled carbon nanotube based nanofluids over a flat plate heater. *Int. J. Heat Mass Transf.* **2011**, *54*, 1289–1296.
11. Hai, T.; Abidi, A.; Wang, L.; Abed, A.M.; Mahmoud, M.Z.; El Din, E.M.T.; Smaisim, G.F. Simulation of solar thermal panel systems with nanofluid flow and PCM for energy consumption management of buildings. *J. Build. Eng.* **2022**, *58*, 104981. [[CrossRef](#)]
12. Shi, M.; Shuai, M.; Chen, Z. Study on pool boiling heat transfer of nanoparticle suspensions on plate surface. *J. Enhanc. Heat Transf.* **2007**, *14*, 223–231. [[CrossRef](#)]
13. Shrivastav, N.; Kashyap, S.; Madan, J.; Al-Mousoi, A.K.; Mohammed, M.K.; Hossain, M.K.; Pandey, R.; Ramanujam, J. Perovskite-CIGS monolithic tandem solar cells with 29.7% efficiency: A numerical study. *Energy Fuels* **2023**, *37*, 3083–3090. [[CrossRef](#)]
14. Ahmad, S.; Ali, K.; Katbar, N.M.; Akhtar, Y.; Cai, J.; Jamshed, W.; El Din, S.M.; Abd-Elmonem, A.; Abdalla, N.S.E. Vortex generation due to multiple localized magnetic fields in the hybrid nanofluid flow—A numerical investigation. *Heliyon* **2023**, *9*, e17756. [[CrossRef](#)] [[PubMed](#)]
15. Norouzipour, A.; Abdollahi, A.; Afrand, M. Experimental study of the optimum size of silica nanoparticles on the pool boiling heat transfer coefficient of silicon oxide/deionized water nanofluid. *Powder Technol.* **2019**, *345*, 728–738. [[CrossRef](#)]
16. Vassallo, P.; Kumar, R. Pool boiling heat transfer experiments in silica-water nanofluids. *Int. J. Heat Mass Transf.* **2004**, *47*, 407–411. [[CrossRef](#)]
17. Hachem, K.; Ansari, M.J.; Saleh, R.O.; Kzar, H.H.; Al-Gazally, M.E.; Altimari, U.S.; Hussein, S.A.; Mohammed, H.T.; Hammid, A.T.; Kianfar, E. Methods of chemical synthesis in the synthesis of nanomaterial and nanoparticles by the chemical deposition method: A review. *BioNanoScience* **2022**, *12*, 1032–1057. [[CrossRef](#)]
18. Das, A.K.; Saha, P. Performance of different structured surfaces in nucleate pool boiling. *Appl. Therm. Eng.* **2009**, *29*, 3643–3653. [[CrossRef](#)]
19. Alimoradi, H.; Shams, M.; Ashgriz, N. Enhancement in the pool boiling heat transfer of copper surface by applying electrophoretic deposited graphene oxide coatings. *Int. J. Multiph. Flow* **2023**, *159*, 104350. [[CrossRef](#)]
20. Alimoradi, H.; Shams, M. Optimization of subcooled flow boiling in a vertical pipe by using artificial neural network and multi objective genetic algorithm. *Appl. Therm. Eng.* **2017**, *111*, 1039–1051. [[CrossRef](#)]
21. Pastuszko, R.; Piasecka, M. Pool boiling on surfaces with mini-fins and micro-cavities. In Proceedings of the 6th European Thermal Sciences Conference, Poitiers, France, 4–7 September 2012.
22. Dadjoo, M.; Etesami, N.; Esfahany, M.N. Influence of orientation and roughness of heater surface on critical heat flux and pool boiling heat transfer coefficient of nanofluid. *Appl. Therm. Eng.* **2017**, *124*, 353–361. [[CrossRef](#)]
23. Alimoradi, H.; Shams, M.; Ashgriz, N. Bubble behavior and nucleation site density in subcooled flow boiling using a novel method for simulating the microstructure of surface roughness. *Korean J. Chem. Eng.* **2022**, *39*, 2945–2958. [[CrossRef](#)]
24. Samawi, K.A.; Abdulrazzaq, S.J.; Zorah, M.; Al-Bahrani, M.; Mahmoud, H.M.; Abdulkareem-Alsultan, G.; Taki, A.G.; Nassar, M.F. MoS₂/graphdiyne nanotube/MXene 3D-interconnected ternary aerogel: A high-performance electrocatalyst for hydrogen evolution reaction. *J. Solid State Chem.* **2024**, *334*, 124690. [[CrossRef](#)]
25. Umesh, V.; Raja, B. A study on nucleate boiling heat transfer characteristics of pentane and CuO-pentane nanofluid on smooth and milled surfaces. *Exp. Therm. Fluid Sci.* **2015**, *64*, 23–29. [[CrossRef](#)]
26. Narayan, P.; Baby, A.K. Survey on nucleate pool boiling of nanofluids: The effect of particle size relative to roughness. *J. Nanoparticle Res.* **2008**, *10*, 1099–1108.
27. Abdollahi, A.; Salimpour, M.R.; Etesami, N. Experimental analysis of magnetic field effect on the pool boiling heat transfer of a ferrofluid. *Appl. Therm. Eng.* **2017**, *111*, 1101–1110. [[CrossRef](#)]
28. Ahmad, J.; González-Lezcano, R.A.; Majdi, A.; Kahla, N.B.; Deifalla, A.F.; El-Shorbagy, M.A. Glass fibers reinforced concrete: Overview on mechanical, durability and microstructure analysis. *Materials* **2022**, *15*, 5111. [[CrossRef](#)]
29. Abdollahi, A.; Salimpour, M.R.; Etesami, N. Experimental analysis of pool boiling heat transfer of ferrofluid on surfaces deposited with nanofluid. *Modares Mech. Eng.* **2016**, *16*, 19–30.
30. Lee, J.H.; Lee, T.; Jeong, Y.H. Experimental study on the pool boiling CHF enhancement using magnetite-water nanofluids. *Int. J. Heat Mass Transf.* **2012**, *55*, 2656–2663. [[CrossRef](#)]
31. Taleghani, M.H.; Khodadadi, S.; Maddahian, R.; Mokhtari-Dizaji, M. Enhancing the bubble collapse energy using the electrohydrodynamic force. *Phys. Fluids* **2023**, *35*, 053316. [[CrossRef](#)]

32. Berger, P.; Adelman, N.B.; Beckman, K.J. Preparation and properties of an aqueous ferrofluid. *J. Chem. Educ.* **1999**, *76*, 943–948. [[CrossRef](#)]
33. Jamed, M.J.; Alhathal Alanezi, A.; Alsahy, Q.F. Effects of embedding functionalized multi-walled carbon nanotubes and alumina on the direct contact poly(vinylidene fluoride-co-hexafluoropropylene) membrane distillation performance. *Chem. Eng. Commun.* **2019**, *206*, 1035–1057. [[CrossRef](#)]
34. Abdulkadhim, A.; Hamzah, H.K.; Ali, F.H.; Abed, A.M.; Abed, I.M. Natural convection among inner corrugated cylinders inside wavy enclosure filled with nanofluid superposed in porous–nanofluid layers. *Int. Commun. Heat Mass Transf.* **2019**, *109*, 104350. [[CrossRef](#)]
35. Abdulkadhim, A.; Hamzah, H.K.; Ali, F.H.; Yıldız, Ç.; Abed, A.M.; Abed, E.M.; Arıcı, M. Effect of heat generation and heat absorption on natural convection of Cu-water nanofluid in a wavy enclosure under magnetic field. *Int. Commun. Heat Mass Transf.* **2021**, *120*, 105024. [[CrossRef](#)]
36. Wang, H.; Habibi, M.; Marzouki, R.; Majdi, A.; Shariati, M.; Denic, N.; Ebid, A.A.K. Improving the self-healing of cementitious materials with a hydrogel system. *Gels* **2022**, *8*, 278. [[CrossRef](#)]
37. Majdi, H.S.; Shubbar, A.A.; Nasr, M.S.; Al-Khafaji, Z.S.; Jafer, H.; Abdulredha, M.; Al Masoodi, Z.; Sadique, M.; Hashim, K. Experimental data on compressive strength and ultrasonic pulse velocity properties of sustainable mortar made with high content of GGBFS and CKD combinations. *Data Brief* **2020**, *31*, 105961. [[CrossRef](#)]
38. Shahnazari, M.R.; Esfandiari, M. Capillary Effects on Surface Enhancement in a Non-Homogeneous Fibrous Porous Medium. *Mech. Adv. Compos. Struct.* **2018**, *5*, 83–90.
39. Wu, S.; Zhu, D.; Li, X. Thermal energy storage behavior of Al₂O₃-H₂O nanofluids. *Thermochim. Acta* **2009**, *483*, 73–77. [[CrossRef](#)]
40. Mohammed, M.K.; Jabir, M.S.; Abdulzahraa, H.G.; Mohammed, S.H.; Al-Azzawi, W.K.; Ahmed, D.S.; Singh, S.; Kumar, A.; Asaithambi, S.; Shekargoftar, M. Introduction of cadmium chloride additive to improve the performance and stability of perovskite solar cells. *RSC Adv.* **2022**, *12*, 20461–20470. [[CrossRef](#)]
41. Pandey, R.; Bhattarai, S.; Sharma, K.; Madan, J.; Al-Mousoi, A.K.; Mohammed, M.K.A.; Hossain, M.K. Halide composition engineered a non-toxic Perovskite-silicon tandem solar cell with 30.7% conversion efficiency. *ACS Appl. Electron. Mater.* **2022**, *5*, 5303–5315. [[CrossRef](#)]
42. Mohammed, M.K.; Al-Mousoi, A.K.; Singh, S.; Younis, U.; Kumar, A.; Dastan, D.; Ravi, G. Ionic liquid passivator for mesoporous titanium dioxide electron transport layer to enhance the efficiency and stability of hole conductor-free perovskite solar cells. *Energy Fuels* **2022**, *36*, 12192–12200. [[CrossRef](#)]
43. Alsultani, M.J.; Abed, H.H.; Ghazi, R.A.; Mohammed, M.A. Electrical Characterization of Thin Films (TiO₂:ZnO)_{1-x}(GO)_x/FTO Heterojunction Prepared by Spray Pyrolysis Technique. *J. Phys. Conf. Ser.* **2020**, *1591*, 012002. [[CrossRef](#)]
44. Esfandiari, M.; Nikan, F.; Shahnazari, M.R. Catalytic pyrolysis of coal particles in a fluidized bed: Experiments and modeling. *Energy Sources Part A Recovery Util. Environ. Eff.* **2017**, *39*, 1478–1483. [[CrossRef](#)]
45. Shubbar, A.A.; Sadique, M.; Nasr, M.S.; Al-Khafaji, Z.S.; Hashim, K.S. The impact of grinding time on properties of cement mortar incorporated high volume waste paper sludge ash. *Karbala Int. J. Mod. Sci.* **2020**, *6*, 7. [[CrossRef](#)]
46. Al-Aaraji NA, H.; Hashim, A.; Hadi, A.; Abduljalil, H.M. Synthesis and enhanced optical characteristics of silicon carbide/copper oxide nanostructures doped transparent polymer for optics and photonics nanodevices. *Silicon* **2022**, *14*, 10037–10044. [[CrossRef](#)]
47. Khodadadi, S.; Taleghani, M.H.; Ganji, D.D.; Gorji-Bandpy, M. Heat transfer enhancement via bubble dynamics along an inclined wall. *Int. Commun. Heat Mass Transf.* **2023**, *145*, 106829. [[CrossRef](#)]
48. Holman, J.P. *Experimental Methods for Engineers*, 8th ed.; McGraw-Hill: New York, NY, USA, 2012; pp. 63–72.
49. Wen, D.; Ding, Y. Experimental investigation into the pool boiling heat transfer of aqueous based Y-alumina nanofluids. *J. Nanoparticle Res.* **2005**, *7*, 265–274. [[CrossRef](#)]
50. Zhang, G.; Ali, Z.H.; Aldlemy, M.S.; Mussa, M.H.; Salih, S.Q.; Hameed, M.M.; Al-Khafaji, Z.S.; Yaseen, Z.M. Reinforced concrete deep beam shear strength capacity modelling using an integrative bio-inspired algorithm with an artificial intelligence model. *Eng. Comput.* **2022**, *38* (Suppl. S1), 15–28. [[CrossRef](#)]
51. Hu, X.; Derakhshanfard, A.H.; Patra, I.; Khalid, I.; Jalil, A.T.; Oplencia, M.J.C.; Dehkordi, R.B.; Toghraie, D.; Hekmatifar, M.; Sabetvand, R. The microchannel type effects on water-Fe₃O₄ nanofluid atomic behavior: Molecular dynamics approach. *J. Taiwan Inst. Chem. Eng.* **2022**, *135*, 104396. [[CrossRef](#)]
52. Al-Majidi, M.H.; Lampropoulos, A.P.; Cundy, A.B.; Tsioulou, O.T.; Alrekabi, S. Flexural performance of reinforced concrete beams strengthened with fibre reinforced geopolymer concrete under accelerated corrosion. In *Structures*; Elsevier: Amsterdam, The Netherlands, 2019; Volume 19, pp. 394–410.
53. Dikshit, M.K.; Singh, S.; Pathak, V.K.; Saxena, K.K.; Agrawal, M.K.; Malik, V.; Salem, K.H.; Khan, M.I. Surface characteristics optimization of biocompatible Ti6Al4V with RCCD and NSGA II using die sinking EDM. *J. Mater. Res. Technol.* **2023**, *24*, 223–235. [[CrossRef](#)]
54. Mahdi, J.M.; Mohammed, H.I.; Talebizadehsardari, P.; Ghalambaz, M.; Majdi, H.S.; Yaïci, W.; Giddings, D. Simultaneous and consecutive charging and discharging of a PCM-based domestic air heater with metal foam. *Appl. Therm. Eng.* **2021**, *197*, 117408. [[CrossRef](#)]
55. Abdulraheem, F.S.; Al-Khafaji, Z.S.; Hashim, K.S.; Muradov, M.; Kot, P.; Shubbar, A.A. Natural filtration unit for removal of heavy metals from water. In *IOP Conference Series: Materials Science and Engineering*; IOP Publishing: Bristol, UK, 2020; Volume 888, p. 012034.

56. Abed, A.M.; Sopian, K.; Mohammed, H.A.; Alghoul, M.A.; Ruslan, M.H.; Mat, S.; Al-Shamani, A.N. Enhance heat transfer in the channel with V-shaped wavy lower plate using liquid nanofluids. *Case Stud. Therm. Eng.* **2015**, *5*, 13–23. [[CrossRef](#)]
57. Parsaee, F.; Fayzullaev, N.; Nassar, M.F.; Abd Alreda, B.; Mahmoud, H.M.; Taki, A.G.; Faraji, M. Co-Fe dual-atom isolated in N-doped graphydine as an efficient sulfur conversion catalyst in Li-S batteries. *J. Alloys Compd.* **2024**, *988*, 174136. [[CrossRef](#)]
58. Mustafa, M.A.; Abdullah, A.R.; Hasan, W.K.; Habeeb, L.J.; Nassar, M.F. Two-Way Fluid-Structure Interaction Study of Twisted Tape Insert in a Circular Tube Having Integral Fins with Nanofluid. *East.-Eur. J. Enterp. Technol.* **2021**, *3*, 111. [[CrossRef](#)]
59. Mourad, A.; Aissa, A.; Abed, A.M.; Smaisim, G.F.; Toghraie, D.; Fazilati, M.A.; Younis, O.; Guedri, K.; Alizadeh, A.A. The numerical analysis of the melting process in a modified shell-and-tube phase change material heat storage system. *J. Energy Storage* **2022**, *55*, 105827. [[CrossRef](#)]
60. Sangeetha, A.; Shanmugan, S.; Alrubaie, A.J.; Jaber, M.M.; Panchal, H.; Attia, M.E.H.; Elsheikh, A.H.; Mevada, D.; Essa, F.A. A review on PCM and nanofluid for various productivity enhancement methods for double slope solar still: Future challenge and current water issues. *Desalination* **2023**, *551*, 116367. [[CrossRef](#)]
61. Al-Farhany, K.; Abdulkadhim, A.; Hamzah, H.K.; Ali, F.H.; Chamkha, A. MHD effects on natural convection in a U-shaped enclosure filled with nanofluid-saturated porous media with two baffles. *Prog. Nucl. Energy* **2022**, *145*, 104136. [[CrossRef](#)]

Disclaimer/Publisher's Note: The statements, opinions and data contained in all publications are solely those of the individual author(s) and contributor(s) and not of MDPI and/or the editor(s). MDPI and/or the editor(s) disclaim responsibility for any injury to people or property resulting from any ideas, methods, instructions or products referred to in the content.